FEBS 30051 FEBS Letters 579 (2005) 6049–6054

Three-dimensional reconstruction of the valyl-tRNA synthetase/elongation factor-1H complex and localization of the δ subunit

Shoulei Jiang[a], Cindy L. Wolfe[b], J. Anthony Warrington[a], Mona Trempe Norcum[a,*]

[a] *Department of Biochemistry, The University of Mississippi Medical Center, 2500 North State Street, Jackson, MS 39216-4505, United States*
[b] *Department of Biology, Tougaloo College, Tougaloo, MS 39174, United States*

Received 28 July 2005; revised 20 September 2005; accepted 26 September 2005

Available online 6 October 2005

Edited by Miguel De la Rosa

Abstract Eukaryotic valyl-tRNA synthetase (ValRS) and the heavy form of elongation factor 1 (EF-1H) are isolated as a stable high molecular mass complex that catalyzes consecutive steps in protein biosynthesis – aminoacylation of tRNA and its transfer to elongation factor. Herein is the first three-dimensional structure of the particle as calculated from electron microscopic images of negatively stained samples of the human ValRS/EF-1H complex. The ca. 12 × 8 nm particle has two distinct domains and each appears to have twofold symmetry. Bound antibodies place two δ subunits near the particle's center. These data support a dimeric head-to-head arrangement of particle components.

Keywords: Aminoacyl-tRNA synthetase; Elongation factor 1; Three-dimensional reconstruction; Protein biosynthesis; Multiprotein complex; Antibody

1. Introduction

Aminoacyl-tRNA synthetases (aaRSs) are a family of enzymes involved in covalent coupling of amino acids with their matching tRNAs [1]. First an aminoacyl adenylate is formed using ATP then the activated amino acid is transferred to the 3′-adenosine of the cognate tRNA. In addition to their role in protein biosynthesis, aaRSs have been found to have alternate activities [2,3]. Examples are transcriptional and translational regulation, synthesis of dinucleotide polyphosphate signaling molecules, tRNA processing, as well as action as cytokines. A feature that is characteristic of several of these enzymes from multicellular eukaryotes is their ability to form large stable complexes [4,5]. To date, two types of aaRS complexes have been described: the "core" multisynthetase complex and the valyl-tRNA synthetase/elongation factor-1H complex (ValRS/EF-1H). These are likely part of highly organized protein biosynthetic machinery in which close association of aaRSs and other protein synthesis factors aids in maximizing speed and accuracy of this essential biological process.

Significant advances have been made in characterization of the multisynthetase complex [6]. This particle contains 11 polypeptides with molecular masses ranging from 18 to 150 kDa. There are nine aaRS activities and three auxiliary proteins (p18, p38 and p43). The three-dimensional structure of the ca. 1.2×10^6 Da complex has been determined by computational microscopy. It is an asymmetric particle V-shaped particle with several openings into the deep central cleft [7]. The internal topography of proteins in the complex has been studied by genetic and biochemical methods [8–12]. The resulting two-dimensional models arrange the components in either two or three domains [11,12]. Recently, a number of relative locations of proteins in the context of the three-dimensional structure of the multisynthetase complex have been accomplished using tRNAs and labeled proteins as structural probes [13].

In contrast, the ValRS/EF-1H complex has been well-studied biochemically, but not structurally. It has been reported that this assembly contains two copies each of ValRS and the "heavy form" of EF-1H and has an overall mass of ca. 700 kDa [14–18]. EF-1H is composed of four subunits: α, β, γ and δ. The normal stoichiometry is one copy of each, although an extra copy of α can be added. When the actual masses of the components as provided by the human protein database (ValRS, 140 kDa; EF-1α, 50 kDa; EF-1β, 24 kDa; EF-1γ, 50 kDa, EF-1δ, 31 kDa) are added, the total mass of the complex in the normal stoichiometry is ca. 600 kDa. This would increase to ca. 700 kDa if an additional copy of the α subunit is included in each EF-1H assembly. Another nomenclature for EF-1H subunits is extant [19] in which the EF-1α, β, γ, δ subunits are named eEF1A, eEF1B$_\alpha$, eEF1B$_\gamma$ and eEF1B$_\beta$, respectively. We have used the traditional nomenclature in order to be consistent with most of the prior studies that have proposed two-dimensional models of the protein arrangements within ValRS/EF-1H complex or of EF-1H alone.

Although the molecular mechanism is not yet known, the biological role of the ValRS/EF-1H complex can be inferred to be a means of facilitating delivery of charged tRNA to the ribosome. That is, ValRS and EF1 couple two consecutive steps of protein biosynthesis. EF-1α forms a ternary complex with aminoacyl-tRNA (aa-tRNA) and GTP to deliver charged tRNAs to the A-site of the ribosome for protein synthesis. The β, γ and δ subunits recycle inactive EF-1α-GDP to the active GTP-bound form by stimulating guanine nucleotide exchange. The GDP/GTP exchange activity is reported to be in the conserved C-terminal domains of β and δ [20,21]. Additionally, EF-1H co-migrates with ribosomes in sucrose gradient centrifugation experiments. This suggests that EF-1βγδ is in close

*Corresponding author. Fax: +1 601 984 1855.
E-mail address: mnorcum@biochem.umsmed.edu (M.T. Norcum).

Abbreviations: aaRS, aminoacyl-tRNA synthetase; ValRS, valyl-tRNA synthetase; EF-1H, four subunit form of elongation factor 1; aa-tRNA, aminoacyl-tRNA

0014-5793/$30.00
doi:10.1016/j.febslet.2005.09.062

proximity to the ribosome and so any free EF-1α/GDP released from the ribosome could immediately react with EF-1βγδ before diffusing into the cytosol [22].

In this study, the first three-dimensional structural information about the ValRS/EF-1H complex is presented. By electron microscopic visualization of bound antibodies, the δ subunit has been localized. This study provides additional evidence that the particle contains two copies of a ValRS/EF-1H protomer and suggests that they are in a head-to-head arrangement. These data form a basis for understanding the functional interaction of ValRS and EF-1H.

2. Materials and methods

2.1. Analytical methods

aaRS activity was measured by the incorporation of [^{14}C]-amino acids into purified *Escherichia coli* tRNA^{val} (Subriden RNA) [23]. Protein concentrations were determined using the Pierce Coomassie Blue protein assay. SDS–PAGE used 10% acrylamide gels prepared according to Laemmli [24]. The protein bands were visualized by silver staining reagents (Bio-Rad) [13]. Mass standards were commercially prepared (Bio-Rad). For immunoblots, proteins were transferred to nitrocellulose (0.2 μm, Schleicher & Schuell). Non-specific protein binding was blocked with 5% non-fat dry milk. A 1:4000 dilution of mouse anti-EF-1α (Upstate USA Inc.) was used as the primary antibody and a 1:25 000 dilution of HRP-conjugated rabbit anti-mouse immunoglobulin (Pierce) was used as the secondary antibody. Detection was performed using the SuperSignal West Pico Chemiluminescent system (Pierce). Gel-filtration HPLC was performed using a 300 × 4.6 mm Bio-Sep-SEC-S 4000 Peek column (Phenomenex) in HPLC buffer (25 mM HEPES, 100 mM NaCl, pH 7.2) with a flow rate of 3.5 ml/min.

2.2. Cell culture and cell-free extract

Human erythroleukemia K562 cells (ATCC #CCL-243) were maintained in Isocoves media or Complete Serum Free media (Mediatech, Inc.) with addition of 5% FBS and 0.5% antibiotic–antimycotic (Invitrogen Corporation). Cells were grown at 37 °C to a concentration of 1.0–3.0 × 10^6 cells/ml, harvested by centrifugation at 1500 × *g* for 20 min and stored as pellets at −80 °C until needed. For lysis, 40-g cells were thawed on ice in 100 ml hypotonic buffer (10 mM HEPES, pH 7.2) which also contained one protease inhibitor cocktail tablet (Roche) per 50 ml. Three additional protease inhibitors were added just prior to use. These were *N*-α-(*p*-toluene sulfonyl)-L-arginine methyl ester (TAME), phenyl methyl sulfonyl fluoride (PMSF) and di-isopropyl fluorophosphate (DIFP) at 1 mM final concentration. After 12 strokes in a Dounce homogenizer, completeness of cell lysis was checked with light microscopy. Cell lysate was then cleared by centrifugation for 20 min at 16 000 × *g*.

2.3. Isolation of ValRS/EF-1H complex

High molecular mass material was extracted from cell lysate by polyethylene glycol (PEG) fractionation. Specifically, 40% PEG 8000 in column buffer (50 mM HEPES, pH 7.2, 5 mM magnesium acetate, 0.5 mM EDTA, 1 mM dithiothreitol, 10% glycerol and the combination of protease inhibitors listed above) was added to lysate to give a final concentration of 5%. After incubation on ice for 60 min, precipitate was collected by centrifugation 20 min at 16 000 × g. This was dissolved in column buffer in preparation for two successive ion exchange chromatography steps. These were a 10 ml column of S-agarose (Bio-Rad) and a 5 ml column of Q-agarose (Bio-Rad). Elution from both columns used a sodium chloride gradient of 100–700 mM. Fractions with high ValRS enzyme activity were combined and stored in aliquots at −20 °C. Immunoblot detection using EF-1α antibody, SDS–PAGE gel patterns and ValRS enzyme activities were used to detect the complex during the purification.

2.4. Electron microscopy

Electron micrographs for three-dimensional reconstruction were obtained of fractions from gel filtration HPLC that were adsorbed onto thin carbon films and stained with either 1% aqueous uranyl acetate or methylamine vanadate (Nanovan™, Nanoprobes, Yaphank, NY) as previously described [23]. Excess antibody was removed from samples that were reacted with rabbit anti-EF-1δ antibodies (Novus Biological Inc.) using gel-filtration HPLC and the fractions were prepared for electron microscopy as above. Electron micrographs were obtained with a LEO912AB transmission electron microscope at 100 kV with absolute magnifications of 63 000. Micrographs were digitized on a flatbed scanner to give a pixel size of 3.2 Å on the image scale.

2.5. Image analysis

The SPIDER/WEB software package was used for all computations [25]. For all reconstructions, images were interactively selected and then aligned using a reference-free algorithm. Calculation of the primary reference structure was from tilt pairs (0°, −54.9°) of micrographs taken with minimum dose focusing. Tilt pairs are used to determine the three Eulerian angles that properly orient the image views for a de novo structure calculation. Uranyl acetate was used as the negative stain at this initial stage in order to maximize image contrast which aided particle selection. After translational and rotational alignment, 560 images were classified using a K-means grouping algorithm. Reconstructions were calculated from appropriately populated classes. Several rounds of merging were done using angles determined by three-dimensional orientation search. The resulting primary reference was refined with 5560 untilted images using projection mapping at 10° intervals.

Final refinement of the structure used 11 206 untilted images of sample negatively stained with methylamine vanadate. Although images have relatively low contrast, additional structural details are typically preserved [7,13]. Angles were again obtained by projection mapping to the primary reference. Care was taken to use the appropriate parameters and number of images in each projection class to prevent introduction of artifacts due to overrepresentation of particular frequencies or views [26]. Resolution limits were determined from the 50% cutoff of the Fourier shell coefficient between reconstructions of half data sets. Thresholds for surface representation were calculated using mass values of 600 and 700 kDa and a partial specific volume of 0.72. Surface representations were created using IRIS EXPLORER (Numerical Algorithms Group, Downers Grove, IL).

3. Results

3.1. Intact ValRS/EF-1H complex was purified to near homogeneity

Gel-filtration HPLC was used as a final purification step for ValRS/EF-1H complex. As shown in Fig. 1A, the main protein peak elutes as high molecular mass material. This provided evidence that the intact dimeric particle had been isolated. To verify that it contained all of the expected components, SDS–PAGE, aminoacylation activity assay and immunoblotting with anti-EF-1α antibody were used to further analyze fractions from the HPLC column. Fig. 1B shows the electrophoretic band patterns of HPLC fractions 24 and 26, which correspond to elution times of 9–10 min. A strong band is seen at the position of 140 kDa. This is the expected mass of ValRS. The two bands with apparent mass of 50 kDa are consistent with the presence of EF-1α and 1γ. The lower two bands of approximately 30 kDa indicate the presence of EF-1β and δ [15,16]. Other protein bands are also visible, e.g., at ca. 200 kDa, which indicates that the complex is not completely purified. However, the amounts of contaminating proteins vary among preparations (data not shown) while the relative ratios of the ValRS/EF-1H complex components are consistent. Additional confirmation of the presence of ValRS was obtained by assaying the fractions for ability to incorporate [^{14}C] valine into tRNA^{val}. As seen in Fig. 1C, enzyme activity peaked at fraction 26. This fraction also contains the peak of EF-1α as determined by immunoblot analysis (Fig. 1D).

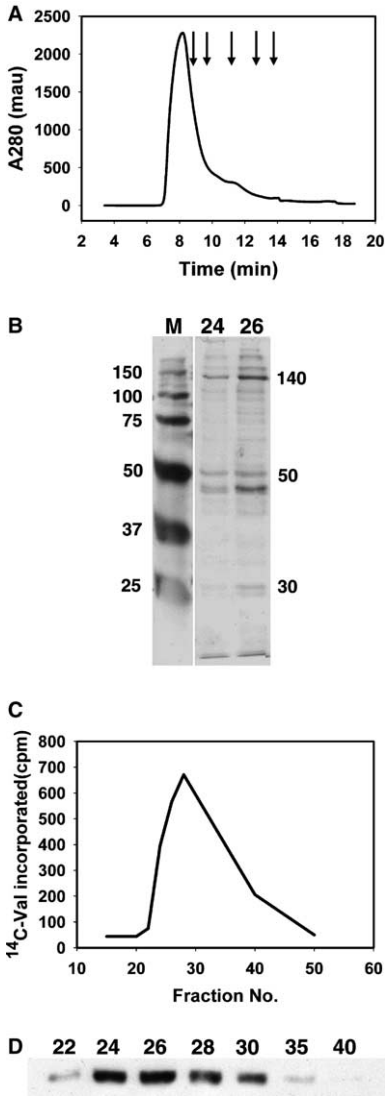

Fig. 1. The isolated ValRS/EF-1H complex is the high molecular mass form and has the appropriate composition. (A) Gel-filtration HPLC indicates that the particle elutes with high molecular mass material. Vertical arrows mark elution times of molecular mass markers. From left to right these are thyroglobulin (670kDa); immunoglobulin G (158 kDa), ovalbumin (44 kDa), myoglobin (17 kDa), Vitamin B-12 (1.35 kDa). (B) Silver stained SDS–PAGE of the peak HPLC fractions shows protein bands of the sizes expected for particle components. Lane 1 is a standard marker. Lanes 2 and 3 are fractions 24 and 26, respectively. (C) The peak of aminoacylation activity coincides with the fractions of appropriate composition and particle size. (D) Immunoblot analysis verifies the presence of the α subunit of EF-1H in the particle.

Earlier studies have established that EF-1H and ValRS activities coelute throughout the isolation procedure used here [16].

Taken together, these results indicate that the isolated particle was indeed the high molecular mass form of the ValRS/EF-1H complex containing two copies of each of ValRS and EF-1H. The key to this purification was inclusion of the protease inhibitor di-isopropyl fluorophosphate (DIFP). Without it, only partial complexes can be isolated. Density gradient ultracentrifugation and electrophoretic analyses demonstrated that these are protomers of one copy each of ValRS tightly associated with EF-1H (data not shown).

3.2. Calculation of the three-dimensional structure of ValRS/EF-1H

Fig. 2A shows a typical electron micrograph of negatively stained ValRS/EF-1H complex after gel filtration HPLC. Although a few larger particles are present, the majority are ca. 12 nm in length. A variety of orientations exists, so the second dimension measurement varies. Most particles are roughly rectangular, although other views are more nearly square and even triangular. Because individual particles are difficult to see as raw data, different particle orientations are demonstrated in Fig. 2B, which shows representative image averages produced by hierarchical classification. The surface representation of the three-dimensional reconstruction is shown below each in an orientation that would produce the observed averages when projected into two dimensions. The selected averages show a two roughly rectangular views and a triangular one. The

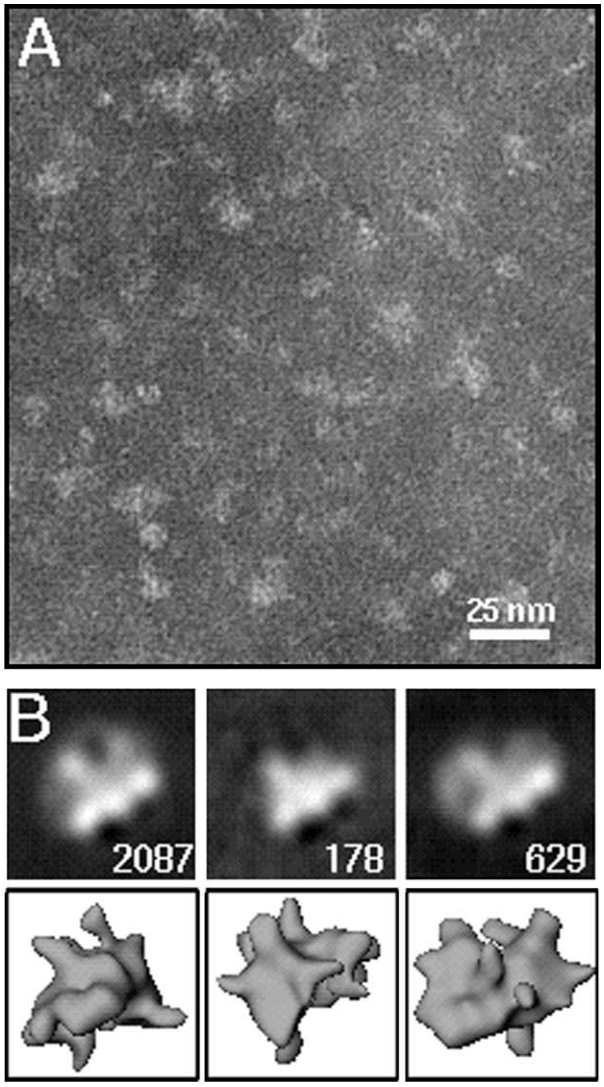

Fig. 2. Electron microscopic images of the ValRS/EF-1H complex are of consistent size but variable orientation. (A) Typical electron micrograph of ValRS/EF-1H complex negatively stained with methylamine vandate. (B) Image averages showing representative particle views (top row) and the three-dimensional reconstruction surface representation in the corresponding orientations (bottom row). The numbers correspond to the number of images in each average.

numbers correspond to the number of images in each average. The average in the third panel composed of 629 images is of particular interest as it suggests the asymmetric two domain structure that is seen in the three-dimensional reconstruction.

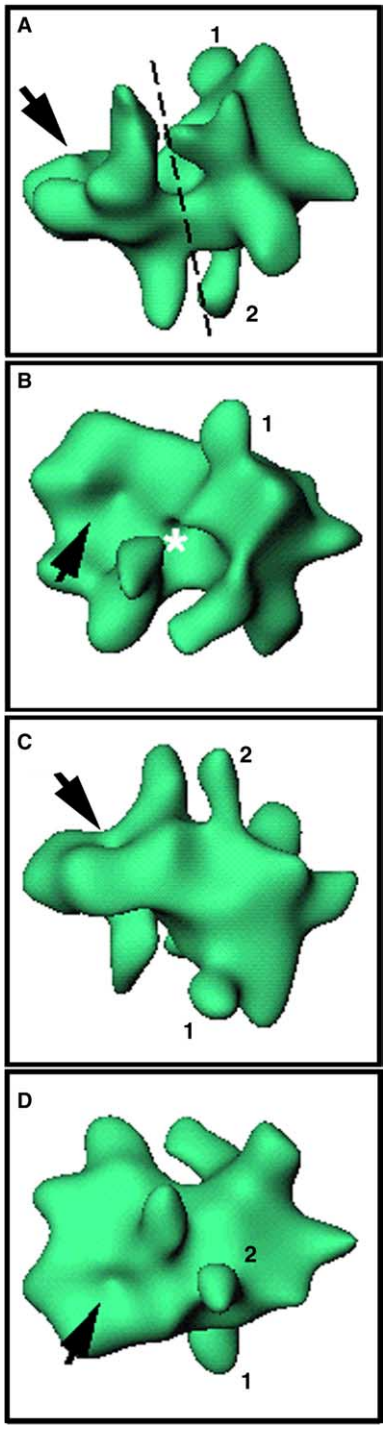

Fig. 3. Surface representation of the refined three-dimensional reconstruction of ValRS/EF-1H complex shows a two-domain assembly. Panels are related by 90° rotations about the horizontal axis. The dotted line (Panel A) denotes the two-domain nature of the reconstruction. Arrows indicate the central depression in the flat domain. Numbers mark two protrusions that are symmetrically arranged in the multi-protrusion domain. Asterisk indicates site where additional density is observed when the threshold is based on a particle mass of 700 kDa.

Fig. 3 shows a surface representation of the final reconstruction of ValRS/EF-1H complex. Refinement of the primary reference with ca. 11 000 images of sample negatively stained with methylamine vanadate resulted in a resolution limit of 30 Å. The overall size is ca. 12×8 nm. Fig. 4A demonstrates that the angular distribution of images chosen for the final reconstruction is complete and that there are no significant over or underrepresentation of particle orientations. Thus, the reconstruction should be free of sampling artifacts.

Each view of the reconstruction in Fig. 3 is related by sequential rotations of 90° about the horizontal axis. The particle can be separated at roughly the midpoint along its long axis (line in panel A) into two domains with very different structural features. One domain consists of a relatively flat section with a central depression (arrows) with two symmetrically

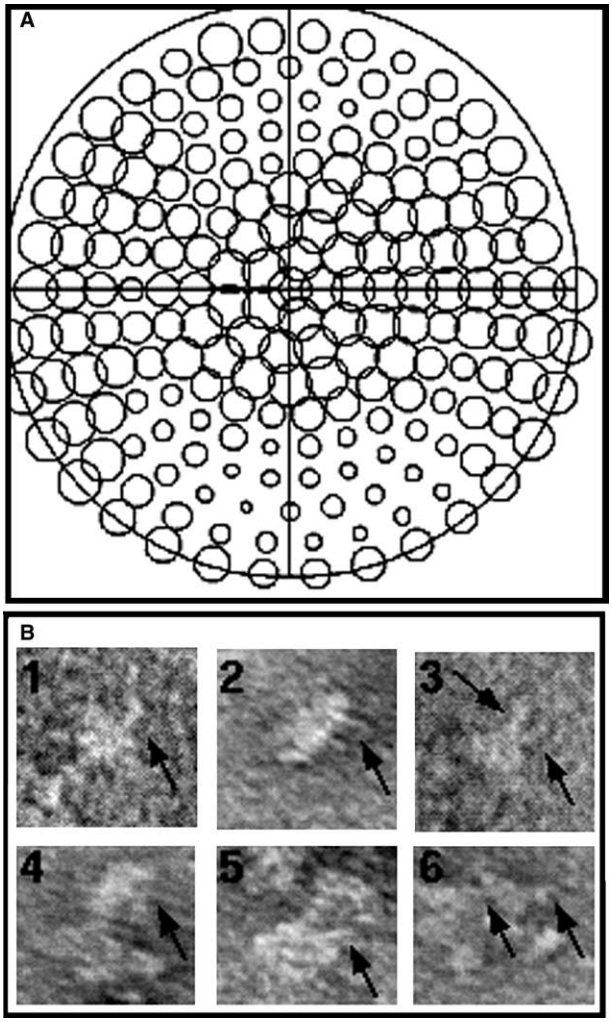

Fig. 4. The data set used for the reconstruction fully covers angular space and visualization of bound antibodies indicates the presence of two copies of the δ subunit near the center of the particle. (A) Plot of angular distribution of images used for the refined reconstruction demonstrates completeness and evenness of the data set. Each circle represents an angular projection of the primary reference structure to which images were mapped. The diameter of each circle increases with the number of images in each projection. (B) Individual electron microscopic images of ValRS/EF-1H complex to which antibodies directed against the δ subunit are bound. Arrows point out the antibody molecules.

arranged protrusions extending above and below. The other domain is characterized by protrusions extending in many directions from the central mass. One can also observe some symmetry in this section as indicated by the extensions labeled 1 and 2, which are on opposite faces of the particle. This feature is best seen in panels A and C. The reconstruction is displayed using a threshold corresponding to the calculated total mass of 600 kDa. If the threshold is determined based on addition of extra copies of EF-1α, extra density is observed forming a connection between two protrusions near the center of the particle as indicated by the asterisk in panel B.

As a first step toward assignment of locations of subunits within the ValRS/EF-1H structure, anti-EF-1δ antibodies were reacted with the complex. After gel-filtration HPLC to remove unbound antibody, samples were negatively stained with uranyl acetate. Fig. 4B consists of a gallery of images in which anti-EF-1δ antibody bound to the complex can be seen (arrows). Panels 1–3 show individual ValRS/EF-1H/antibody complexes and panels 4–6 show multiple particles that appear linked by antibodies. As is best seen in panels 1 and 4, the site of antibody binding is near the center of the long axis of the particle. This places the δ subunit at or near the intersection of the two domains of the complex. Panels 3 and 6 show simultaneous binding of two antibodies. This indicates the presence of at least two copies of the δ subunit and supports dimeric models of the complex.

4. Discussion

Several two-dimensional models have been proposed for relative placement of the components within the ValRS/EF-1H complex or within EF-1H alone. These are based on interactions obtained by in vitro biochemical studies including reconstitution experiments, site-directed mutagenesis and limited protease cleavage [18,22,27]. There is much inconsistency among these two-dimensional models. For example, from in vitro reconstitution experiments, an EF-1H stoichiometry of $\alpha_2\beta\gamma\delta$ has been proposed [22]. Both subunits β and δ were shown as binding to the same γ subunit, but to different α subunits. Based on protein kinase CKII phosphorylation sites [27], a model for the ValRS/EF-1H complex was developed in which the particle consists of $(\alpha_2\beta\gamma\delta\text{ValRS})_2$. The N-terminal extension of each EF-1δ would bind to the N-terminal hydrophobic extension of ValRS, which is known to mediate its association with EF-1H [28]. The major difference between these two models is the presence of β and γ dimers in the second model. In contrast, the model proposed by Bec et al. [18] was based on a δ dimer in the core held together by the leucine zipper motif in the subunits N-terminii. Also, each δ subunit is shown binding to a γ subunit. The β subunit alone interacts with an α and a γ subunit, while the δ subunit interacts with ValRS to form $(\alpha\beta\gamma\delta\text{ValRS})_2$. This model is different from that proposed by Sheu and Traugh [27] with regard to formation of the δ dimer and lack of association of a δ and an α subunit.

The cartoon in Fig. 5 incorporates the data from this study with that described above. The model shown is composed of two ValRS/EF1-H protomers. The antibody binding sites observed (Fig. 4B) adds to the evidence that the δ subunits are at or near the center of the ValRS/EF-1H complex. The remaining EF-1H subunits are placed to take into account the associations described above. ValRS is located at one end based on the reported direct interaction with the δ subunit. Both ValRS and the EF-1α subunits are on the exterior of the model as is logical for their need to be readily accessible to substrates. This placement is also consistent with the ability of antibodies directed against the α subunit to bind to this subunit in the native ValRS/EF-1H complex as demonstrated by immunoblot analysis (data not shown). The protomers are placed in a head-to-head arrangement due to the marked morphological differences between the two domains in the three-dimensional reconstruction (Fig. 3).

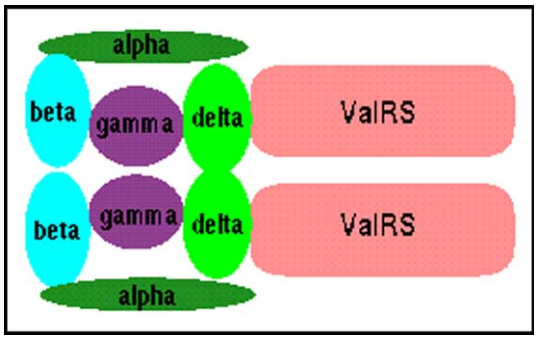

Fig. 5. Cartoon of the components of the ValRS/EF-1H complex showing the two-domain nature of the assembly and a head-to-head arrangement of the protomers. Placements of the EF-1H subunits take into account the antibody binding data from this study and the contacts detected by others using a variety of biochemical methods as described in the text.

The combination of the three-dimensional structural information presented in this study with previous biochemical studies also provides some insight into the function of the ValRS/EF-1H complex. That is, when the reconstruction threshold is recalculated to accommodate extra EF-1α subunits (Fig. 3B) the additional mass observed is near the center of the particle and appears only on one side. Although there is some uncertainty about the significance of this change at the current level of resolution of the reconstruction, this would suggest that EF-1α and ValRS are close to one another. This would facilitate formation of the ternary complex of valyl-tRNA, GTP and EF-1α. As EF-1α is rather loosely bound to the complex [29], it can then readily deliver charged valyl-tRNA to the ribosome. Thus, coupling two consecutive reactions in one particle contributes to the high efficiency of protein biosynthesis.

Higher resolution structures and additional protein localizations are needed to clearly distinguish among the many models of the component arrangements within the ValRS/EF-1H complex. However, understanding the structure and function of the ValRS/EF-1H complex is a fundamental part in understanding of eukaryotic protein biosynthesis at the molecular level. It also bears on the elucidation of the principles underlying intracellular organization. It is notable that the strength of interaction of ValRS with EF1 is much weaker in bacteria than in eukaryotes [15] and no complex of the two is known to exist. Thus, study of the ValRS/EF-1H complex may provide additional means of distinguishing between the mechanisms of regulation of protein synthesis and other complex cellular processes in bacteria from those in eukaryotes.

Acknowledgments: We are grateful to Angela Reiken for her contributions in editing the manuscript. This work was supported by the National Science Foundation through Grant Nos. MCB-0090539 and MCB-0215940.

References

[1] Schimmel, P.R. and Söll, D. (1979) Aminoacyl-tRNA synthetases: general features and recognition of transfer RNAs. Ann. Rev. Biochem. 48, 601–648.

[2] Francklyn, C., Musier-Forsyth, K. and Martinis, S.A. (1997) Aminoacyl-tRNA synthetases in biology and disease: new evidence for structural and functional diversity in an ancient family of enzymes. RNA 3, 954–960.

[3] Martinis, S.A., Plateau, P., Cavarelli, J. and Florentz, C. (1999) Aminoacyl-tRNA synthetases: a family of expanding functions. EMBO J. 18, 4591–4596.

[4] Kisselev, L.L. and Wolfson, A.D. (1994) Aminoacyl-tRNA synthetases from higher eukaryotes. Prog. Nucl. Acc. Res. Mol. Biol. 48, 83–142.

[5] Yang, D.C.H. (1996) Mammalian aminoacyl-tRNA synthetases. Curr. Top. Cell Reg. 34, 101–136.

[6] Han, J.M., Kim, J.Y. and Kim, S. (2003) Molecular network and functional implications of macromolecular tRNA synthetase complex. Biochem. Biophys. Res. Commun. 303, 985–993.

[7] Wolfe, C.L., Warrington, J.A., Davis, S., Green, S. and Norcum, M.T. (2003) Isolation and characterization of human nuclear and cytosolic multisynthetase complexes and the intracellular distribution of p43/EMAP II. Protein Sci. 12, 2282–2290.

[8] Rho, S.B., Kim, M.J., Lee, J.S., Seol, W., Motegi, H., Kim, S. and Shiba, K. (1999) Genetic dissection of protein–protein interactions in multi-tRNA synthetase complex. Proc. Natl. Acad. Sci. USA 93, 4488–4493.

[9] Quevillon, S., Robinson, J.-C., Berthonneau, E., Siatecka, M. and Mirande, M. (1999) Macromolecular assemblage of aminoacyl-tRNA synthetases: identification of protein–protein interactions and characterization of a core protein. J. Mol. Biol. 285, 183–195.

[10] Robinson, J.-C., Kerjan, P. and Mirande, M. (2000) Macromolecular assemblage of aminoacyl-tRNA synthetases: quantitative analysis of protein–protein interactions and mechanism of complex assembly. J. Mol. Biol. 304, 983–994.

[11] Kim, J.Y., Kang, Y.-S., Lee, J.-W., Kim, H.J., Ahn, Y.H., Park, H., Ko, Y.-G. and Kim, S. (2002) p38 is essential for the assembly and stability of macromolecular tRNA synthetase complex: implications for its physiological significance. Proc. Natl. Acad. Sci. USA 99, 7912–7916.

[12] Norcum, M.T. and Warrington, J.A. (1998) Structural analysis of the multienzyme aminoacyl-tRNA synthetase complex: a three-domain model based on reversible chemical crosslinking. Protein Sci. 7, 79–87.

[13] Wolfe, C.L., Warrington, J.A., Treadwell, L. and Norcum, M.T. (in press) A three-dimensional working model of the multienzyme complex of aminoacyl-tRNA synthetases based on electron microscopic placements of tRNA and proteins. J. Biol. Chem. Available online: doi:10.1074/jbc.M502759200.

[14] Motorin, Y.A., Wolfson, A.D., Orlovsky, A.F. and Gladilin, K.L. (1987) Purification of valyl-tRNA synthetase high-molecular-mass complex from rabbit liver. FEBS Lett. 220 (2), 363–365.

[15] Bec, G., Kerjan, P., Zha, X.D. and Waller, J.-P. (1989) Valyl-tRNA synthetase from rabbit liver. I. Purification as a heterotypic complex in association with elongation factor 1. J. Biol. Chem. 264 (35), 21131–21137.

[16] Motorin, Y.A., Wolfson, A.D., Löhr, D., Orlovsky, A.F. and Gladilin, L. (1991) Purification and properties of a high-molecular-mass complex between val-tRNA synthetase and the heavy form of elongation factor 1 from mammalian cells. Eur. J. Biochem. 201, 325–331.

[17] Venema, R.C., Peters, H.I. and Traugh, J.A. (1991) Phosphorylation of elongation factor 1 (EF-1) and valyl-tRNA synthetase by protein kinase C and stimulation of EF-1 activity. J. Biol. Chem. 266, 12574–12580.

[18] Bec, G., Kerjan, P. and Waller, J.P. (1994) Reconstitution in vitro of the valyl-tRNA synthetase-elongation factor (EF) 1βγδ complex. J. Biol. Chem. 269 (3), 2086–2092.

[19] Mansilla, F., Friis, I., Jadidi, M., Nielsen, K.M., Clark, B.F.C. and Knudsen, C.R. (2002) Mapping the human translation elongation factor eEF1H complex using the yeast two-hybrid system. Biochem. J. 365, 669–676.

[20] Van Damme, H.T., Amons, R., Karssies, R., Timmers, C.J., Janssen, G.M. and Moller, W. (1990) Elongation factor 1β of Artemia: localization of functional sites and homology to elongation factor 1δ. Biochem. Biophys. Acta 1050, 241–247.

[21] Sanders, J., Raggiaschi, R., Morales, J. and Moller, W. (1993) The human leucine-zipper containing guanine-nucleotide exchange protein elongation factor-1δ. Biochim. Biophys. Acta 1174, 87–90.

[22] Janssen, G.M., van Damme, H.T.F., Kriek, J., Amons, R. and Möller, W. (1994) The subunit structure of elongation factor 1 from *Artemia*. Why two α-chains in this complex?. J. Biol. Chem. 269 (50), 31410–31417.

[23] Norcum, M.T. (1989) Isolation and electron microscopic characterization of the high molecular mass aminoacyl-tRNA synthetase complex from murine erythroleukemia cells. J. Biol. Chem. 264, 15043–15051.

[24] Laemmli, U.K. (1970) Cleavage of structural proteins during the assembly of the head of bacteriophage T4. Nature 227, 680–685.

[25] Frank, J., Radermacher, M., Penczek, P., Zhu, J., Li, Y.H., Ladjadj, M. and Leith, A. (1996) SPIDER and WEB: Processing and visualization of images in 3D electron microscopy and related fields. J. Struct. Biol. 116, 190–199.

[26] Sorzano, C.O., Marabini, R., Boisset, N., Rietzel, E., Schroder, R., Herman, G.T. and Carazo, J.M. (2001) The effect of overabundant projection directions on 3D reconstruction algorithms. J. Struct. Biol. 133, 108–118.

[27] Sheu, G.-T. and Traugh, J.A. (1999) A structural model for elongation factor 1 (EF-1) and phosphorylation by protein kinase CKII. Mol. Cell. Biochem. 191, 181–186.

[28] Hsieh, S.L. and Campbell, R.D. (1991) Evidence that gene G7a in the human major histocompatibility complex encodes valyl-tRNA synthetase. Biochem. J. 278, 809–816.

[29] Negrutskii, B.S., Shalak, V.F., Kerjan, P., El' skaya, A.V. and Mirande, M. (1999) Functional interaction of mammalian valyl-tRNA synthetase with elongation factor EF-1α in the complex with EF-1H. J. Biol. Chem. 274, 4545–4550.